The Astrophysical Journal, 953:125 (8pp), 2023 August 20 https://doi.org/10.3847/1538-4357/ace18e

An Ongoing Tidal Capture in the Large Magellanic Cloud: The Low-mass Star Cluster KMK 88-10 Captured by the Massive Globular Cluster NGC 1835?*

Camilla Giusti[1,2], Mario Cadelano[1,2], Francesco R. Ferraro[1,2,4], Barbara Lanzoni[1,2], Silvia Leanza[1,2], Cristina Pallanca[1,2], Enrico Vesperini[3], Emanuele Dalessandro[2], and Alessio Mucciarelli[1,2]
[1] Dipartimento di Fisica e Astronomia, Università degli Studi di Bologna, via Gobetti 93/2, I-40129 Bologna, Italy; francesco.ferraro3@unibo.it
[2] INAF—Astrophysics and Space Science Observatory Bologna, Via Gobetti 93/3, I-40129, Bologna, Italy
[3] Department of Astronomy, Indiana University, Bloomington, IN 47401, USA
Received 2023 April 28; revised 2023 June 22; accepted 2023 June 22; published 2023 August 10

Abstract

In the context of a project aimed at characterizing the dynamical evolution of old globular clusters in the Large Magellanic Cloud, we have secured deep HST/WFC3 images of the massive cluster NGC 1835. In the field of view of the acquired images, at a projected angular separation of approximately 2′ from the cluster, we detected the small stellar system KMK 88-10. The observations provided the deepest color–magnitude diagram ever obtained for this cluster, revealing that it hosts a young stellar population with an age of 600–1000 Myr. The cluster surface brightness profile is nicely reproduced by a King model with a core radius $r_c = 4''$ (0.97 pc), a half-mass radius $r_{hm} = 12''$ (2.9 pc), and a concentration parameter $c \sim 1.3$ corresponding to a truncation radius $r_t \sim 81''$ (19.5 pc). We also derived its integrated absolute magnitude ($M_V = -0.71$) and total mass ($M \sim 80$–$160\ M_\odot$). The most intriguing feature emerging from this analysis is that KMK 88-10 presents a structure elongated in the direction of NGC 1835, with an intracluster overdensity that suggests the presence of a tidal bridge between the two systems. If confirmed, this would be the first evidence of a tidal capture of a small star cluster by a massive globular.

Unified Astronomy Thesaurus concepts: Stellar photometry (1620); Young star clusters (1833); Large Magellanic Cloud (903)

1. Introduction

The Large Magellanic Cloud (LMC) is the closest (irregular) galaxy to the Milky Way (MW). Due to its proximity (∼50 kpc; Harris & Zaritsky 2009; Pietrzyński et al. 2019), it is possible to resolve individual stars even within its stellar clusters. These are rich star clusters, with properties similar to those of the MW globular clusters and lower-mass systems resembling the Galactic open clusters. At odds with their Galactic counterparts, globular clusters in the LMC exhibit a wide range of ages (from a few million to several billion years), thus providing a unique laboratory to study the major changes in the observational properties of stellar populations as a function of age (see, e.g., Ferraro et al. 1995, 2004; Mucciarelli et al. 2006). Moreover, they provide deep insights into the LMC star formation history (Baumgardt et al. 2013) and chemical enrichment (e.g., Pietrzynski & Udalski 2000; Glatt et al. 2010). While these systems have been targeted in several studies through the years (e.g., Brocato et al. 1996; Olsen et al. 1998; Mackey & Gilmore 2003; Ferraro et al. 2006; Mucciarelli et al. 2008, 2010; Ferraro et al. 2019; Lanzoni et al. 2019; Cadelano et al. 2022), an extensive and comprehensive study of LMC low-mass clusters is still lacking. This is because they are composed of a limited number of stars embedded in the LMC field population, which severely hinders their detection and makes them easily misidentifiable with asterisms (Bica et al. 2008; Choudhury et al. 2015; Nayak et al. 2016). Nevertheless, such systems are crucial for understanding the formation and evolution of the LMC (Piatti 2012; Palma et al. 2013; Piatti et al. 2014; Choudhury et al. 2015; Palma et al. 2016).

Interestingly, "star cluster pairs" with small projected relative distances are frequently observed in the LMC (Priyatikanto et al. 2019, 2019). Bhatia & Hatzidimitriou (1988), Bhatia et al. (1991), Subramaniam et al. (1995), and Dieball et al. (2002) used statistical arguments to prove that the large number of observed cluster pairs cannot be fully explained by random projection effects. This indicates that at least some of them are likely gravitationally bound, and observational confirmations of this hypothesis have been found in a few cases (e.g Mucciarelli et al. 2012; De Silva et al. 2015; Dalessandro et al. 2018). Interacting binary clusters could be the result of the primordial fragmentation of a common molecular cloud or the outcome of a close encounter between two clusters during their motion in the galaxy and a subsequent tidal capture (see, e.g., Dieball et al. 2002; Mucciarelli et al. 2012; Dalessandro et al. 2018). While in the former case, binary clusters are expected to share some common properties (such as age and chemical composition), in the latter case, the two members can have very different ages, masses, and chemical abundances.

Cluster pairs generated by encounter processes can bring a wealth of information about the evolutionary history of the host galaxy, as well as explain the properties of individual systems with peculiar characteristics, such as unusual rotation patterns (Lee et al. 1999; Baumgardt et al. 2003; Brüns & Kroupa 2011) or spreads in chemical abundances (e.g., Amaro-Seoane et al. 2013; Gavagnin et al. 2016; Hong et al. 2017). For this reason, they have been extensively studied in the past, mainly through *N*-body simulations (Rao et al. 1987; de Oliveira et al. 1998, 2000; Portegies Zwart & Rusli 2007; de la Fuente

* Based on observations collected at the Hubble Space Telescope under proposal GO16361 (PI: Ferraro).
[4] Corresponding author.

Marcos & de la Fuente Marcos 2010; Priyatikanto et al. 2016; Darma et al. 2021). The fate of these systems seems to be twofold; those having a small initial separation will likely experience a merger in a relative short timescale, while the ones with a larger initial separation will probably be moved apart by the tidal forces of the host galaxy (Darma et al. 2021). Tidal captures are expected to occur more often in dwarf galaxies such as the LMC, rather than in the MW, due to a smaller relative velocity of star clusters (van den Bergh 1996). In spite of this, the encounter rate per cluster in the LMC is predicted to be quite low ($dN/dt \sim 10^{-9}$ yr; Vallenari et al. 1998), making the possibility of an encounter highly unlikely for very young clusters.

In this paper, we provide the first tentative evidence of an ongoing tidal capture of the small star cluster KMK 88-10 by the massive globular cluster NGC 1835 in the LMC. This study is part of a project aimed at characterizing the dynamical age of old stellar clusters in the LMC (Ferraro et al. 2019; Lanzoni et al. 2019) by using the so-called "dynamical clock" (see Ferraro et al. 2012; Lanzoni et al. 2016; Ferraro et al. 2018, 2020, 2023). To this end, we secured a set of multiband Hubble Space Telescope (HST) images of NGC 1835, a very massive ($\sim 6 \times 10^5\ M_\odot$; Mackey & Gilmore 2003; McLaughlin & van der Marel 2005), old ($t \sim 13$ Gyr; Olsen et al. 1998), and metal-poor ([Fe/H] ~ -1.7 dex; Mucciarelli et al. 2021) globular cluster lying close to the central bar of the LMC. Near the border of the sampled field of view, a small and loosely populated star cluster is clearly visible; this is KMK 88-10 (also called H88 120 and OGLE-CL LMC 74; see Narloch et al. 2022). It was first identified by Pietrzynski & Udalski (2000) and later studied by Bica et al. (2008), Nayak et al. (2016), and Narloch et al. (2022), who estimated a very low mass ($\sim 300\ M_\odot$) and young age ($t \sim 500$ Myr). However, its characteristics have never been investigated in depth with adequate high-resolution and deep observations. Thanks to the acquired data set, here we provide a detailed characterization of this stellar system and probe the possibility that it is experiencing a physical interaction with NGC 1835. In agreement with the considerations above about the encounter rate per cluster in the LMC, very few cases of this kind are known observationally, and no evidence of ongoing tidal captures between systems with very different ages and extremely high mass ratios ($M_1/M_2 \geqslant 10^3$) has been collected so far. Only theoretical simulation studies are available (de la Fuente Marcos et al. 2014), predicting that such interactions should lead to tidal destruction and/or accretion of the lower-mass system (secondary) by the higher-mass one (primary). A stellar overdensity in the region connecting the two clusters (de Oliveira et al. 1998; Leon et al. 1999) and dynamical heating of the stars in the outer regions of the primary are also expected (Rao et al. 1987; de la Fuente Marcos et al. 2014).

The paper is organized as follows. In Section 2, we describe the data set and data reduction process. In Section 3, we present the determination of the age and structural parameters of the cluster. In Section 4, we investigate the possibility of an ongoing tidal interaction between KMK 88-10 and NGC 1835. The summary and discussion of the results are provided in Section 5.

2. Data Set and Data Reduction

The adopted data set consists of deep and high-resolution images obtained with the Wide Field Camera 3 (WFC3) on board the HST under program GO 16361 (PI: Ferraro). A total of 16 images were collected with different filters: six images in the ultraviolet (UV) filter F300X with exposure times ranging from 917 to 953 s, six in F606W with an exposure time of 408 s, and four in F814W with exposure times ranging from 630 to 700 s. For decontamination purposes, as part of the same program, a set of simultaneous parallel observations with the Wide Field Camera of the Advanced Camera for Surveys (ACS) have been secured in the F606W and F814W filters to sample a region of the LMC located $\sim 5'$ from the WFC3 pointing. The data of NGC 1835 presented in this paper were obtained from the Mikulski Archive for Space Telescopes at the Space Telescope Science Institute. The specific observations analyzed can be accessed via DOI:10.17909/d4qh-wq06.

The data reduction has been performed with the software DAOPHOT IV (Stetson 1987), following the recipes described in detail in Cadelano et al. (2019, 2020, 2020). The first step consisted of the modeling of a spatially varying point-spread function (PSF) in each image, and, for this purpose, approximately 200 bright, isolated, and well-distributed stars were selected and analyzed. Subsequently, we identified all of the sources with a flux peak above 5σ from the level of the background, and we fitted the PSF models previously found to all of these detected sources. Using as reference a master list including the stars identified in at least half of the images acquired with the UV filter, we forced the fit of the PSF model to the location of these sources in all of the other images using DAOPHOT/ALLFRAME (Stetson 1994). For each of the identified stars, the magnitude values estimated in different images were combined using DAOMATCH and DAOMASTER. The final catalog contains detector positions, instrumental magnitudes, and photometric errors for about 65,000 sources. The magnitudes were then calibrated onto the VEGAMAG photometric system, applying the appropriate aperture corrections and zero-points reported on the HST WFC3 website.[5] The instrumental positions were corrected for geometric distortion effects using the correction coefficients quoted in Bellini et al. (2011). Finally, we transformed the corrected positions to the absolute coordinate system (α, δ) by cross-correlation with the Gaia DR3 catalog (Gaia Collaboration et al. 2022).

3. Analysis

As anticipated in Section 1, the main target of the acquired HST observations was NGC 1835. Hence, one of the two chips of the WFC3 was roughly centered on the cluster center (see Figure 1). During the analysis, we detected an overdensity of stars located at the northern edge of the field of view resembling a small stellar cluster. By cross-correlating its position with the SIMBAD catalog (Wenger et al. 2000), we identified this overdensity as the star cluster KMK 88-10. While the photometric properties of the main target (NGC 1835) will be presented in a companion paper (C. Giusti et al. 2023, in preparation), here we discuss the characteristics of KMK 88-10 as derived from the analysis of this data set. Figure 1 shows one of the secured images in the F814W band, with the positions of both KMK 88-10 and NGC 1835 highlighted. Interestingly, the two stellar systems are separated by a projected distance of about 130″, which is only slightly

[5] https://www.stsci.edu/hst/instrumentation/wfc3/data-analysis/photometric-calibration/uvis-photometric-calibration

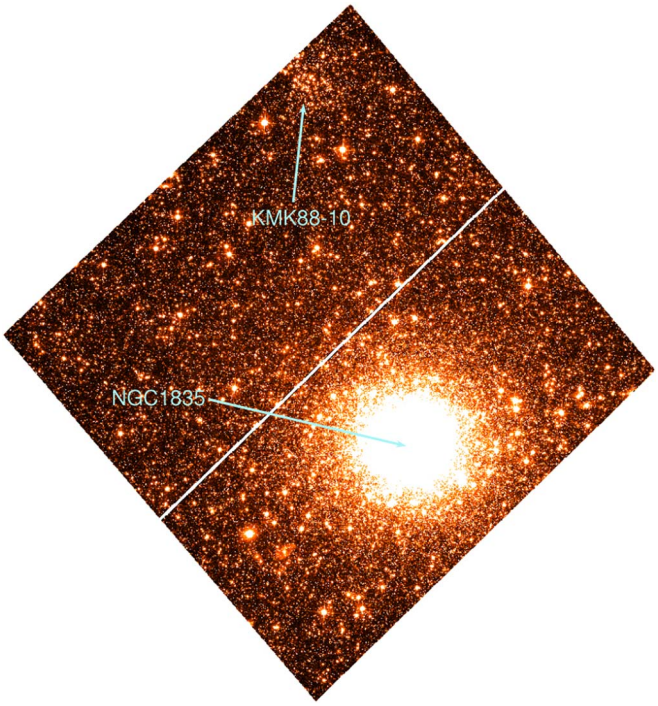

Figure 1. The HST/WFC3 image in the F814W filter showing the positions of KMK 88-10 and NGC 1835. The field of view is 160″ × 160″. North is up, and east is left.

larger than the tidal radius of NGC 1835 of ∼105″ (C. Giusti et al. 2023, in preparation; McLaughlin & van der Marel 2005).

3.1. Decontamination of the Color–Magnitude Diagram

The optical color–magnitude diagram (CMD) of a circular region with a radius of 15″ centered on KMK 88-10 is shown in Figure 2(a). The radius was chosen as the best compromise between including most of the cluster stars and, at the same time, minimizing the number of field interlopers. Down to magnitude $m_{\rm F606W} = 24$, this area includes 701 stars. The CMD shows a very extended main sequence (MS), ranging from $m_{\rm F606W} \sim 18.4$ to 25.5. An extended and well-defined red giant branch (RGB) occupies the region at magnitude $18.2 < m_{\rm F606W} < 22$ and color $0.5 < m_{\rm F606W} - m_{\rm F814W} < 0.9$. For comparison, in Figure 2(b), we show the CMD of an LMC field region of the same size, selected beyond the tidal radius of NGC 1835. From an immediate visual comparison between the cluster and the field CMDs, it appears evident that the extended RGB visible in panel (a) can be almost entirely attributed to the old field population, while the small clump of stars at $m_{\rm F606W} = 18.5$ seems to be present only in KMK 88-10. The brightest portion of the MS ($m_{\rm F606W} < 20$) also appears to be a component not present in the field. The selected reference field area contains 409 stars down to magnitude $m_{\rm F606W} = 24$. Thus, we can roughly estimate that the overall contribution of LMC field stars in the direction of KMK 88-10 down to $m_{\rm F606W} = 24$ is as large as ∼58%. This clearly indicates that a proper decontamination of the CMD of KMK 88-10 from the field contribution is mandatory to perform a detailed characterization of the cluster properties.

A decontamination through proper motions would be very challenging at the large distances of the LMC (see, e.g., Cadelano et al. 2022), and in this case, it is not feasible at all because of the lack of a second epoch of observations. We therefore applied a statistical decontamination technique, following an approach similar to that proposed in Milone et al. (2018; see also Dalessandro et al. 2019). For each star observed in the reference field, we removed one star from the cluster sample selected on the basis of its relative position in the CMD. More specifically, for each ith star in the reference field, we calculated its CMD distance (d_i)[6] from all of the stars belonging to the cluster sample. Then, we selected as the most likely interloper stars in the cluster sample the objects having the lowest values of d_i. Thus, by construction, the procedure returns 409 field interlopers and 292 likely cluster member stars. The entire process was repeated several times using different reference fields of equal size. All of the decontaminated CMDs thus obtained are qualitatively in agreement, confirming that the adopted procedure provides reliable results. An example of a decontaminated CMD obtained with this approach is shown in Figures 2(c)–(e) for all of the filter combinations. As is apparent, an extended MS survived the selection, indicating the existence of a young population with an MS turnoff point at $m_{\rm F606W} \approx 19$. A small clump of objects at the position of the red clump of this young population also remained in the cluster sample; see the stars located at an average magnitude of $m_{\rm F606W} \sim 18.5$ and color $(m_{\rm F606W} - m_{\rm F814W}) \sim 0.7$. As expected, most of the stars along the RGB have been removed. The only exceptions are four red objects with colors $0.8 < (m_{\rm F606W} - m_{\rm F814W}) < 0.95$ and magnitudes $18 < m_{\rm F606W} < 19.5$, which are most likely residual field stars that survived the decontamination process due to the low statistics along the bright portion of the LMC RGB.

3.1.1. The Cluster Age

To estimate the cluster age, we compared the decontaminated CMD with a set of isochrones from the PARSEC database (Marigo et al. 2017). We extracted isochrones at different ages (between 600 and 1000 Myr) assuming a metallicity [Fe/H] = −0.4 dex, which is typical for the young LMC stellar population (Mucciarelli et al. 2008) and compatible with that derived by Narloch et al. (2022), who quoted a value ranging between −0.52 and −0.44 dex. We also adopted a color excess of $E(B-V) = 0.06$.[7]

Finally, we adopted the LMC distance modulus $(m-M)_0 = 18.48$, corresponding to a distance of 49.6 kpc (Pietrzyński et al. 2019). In Figure 3, we show the decontaminated optical and hybrid ($m_{\rm F814W}$, $m_{\rm F300X} - m_{\rm F814W}$) CMDs. As can be seen, the MS turnoff region appears broadened in color, as commonly observed in young star clusters and likely due to the effects of stellar rotation (Mackey & Broby Nielsen 2007; Kamann et al. 2020; Martocchia et al. 2023) and the presence of MS binaries. This hampers a solid determination of the cluster age, as rotating stars can be brighter or fainter than nonrotating stars depending on their angular velocities and inclination angles with respect to the observer. However, the comparison with isochrones for

[6] The CMD distance between a star belonging to the cluster sample and the ith star of the reference field is defined as $d_i = \sqrt{(\mathrm{COL}_c - \mathrm{COL}_f)^2 + (\mathrm{MAG}_c - \mathrm{MAG}_f)^2}$, where COL_c and COL_f are the ($m_{\rm F606W} - m_{\rm F814W}$) colors of the stars in the cluster and field samples, respectively, while MAG_c and MAG_f are the corresponding values of their F606W magnitude.

[7] We refer the reader to the forthcoming paper about NGC 1835 in which we will independently derive the $E(B-V)$ of the analyzed field of view.

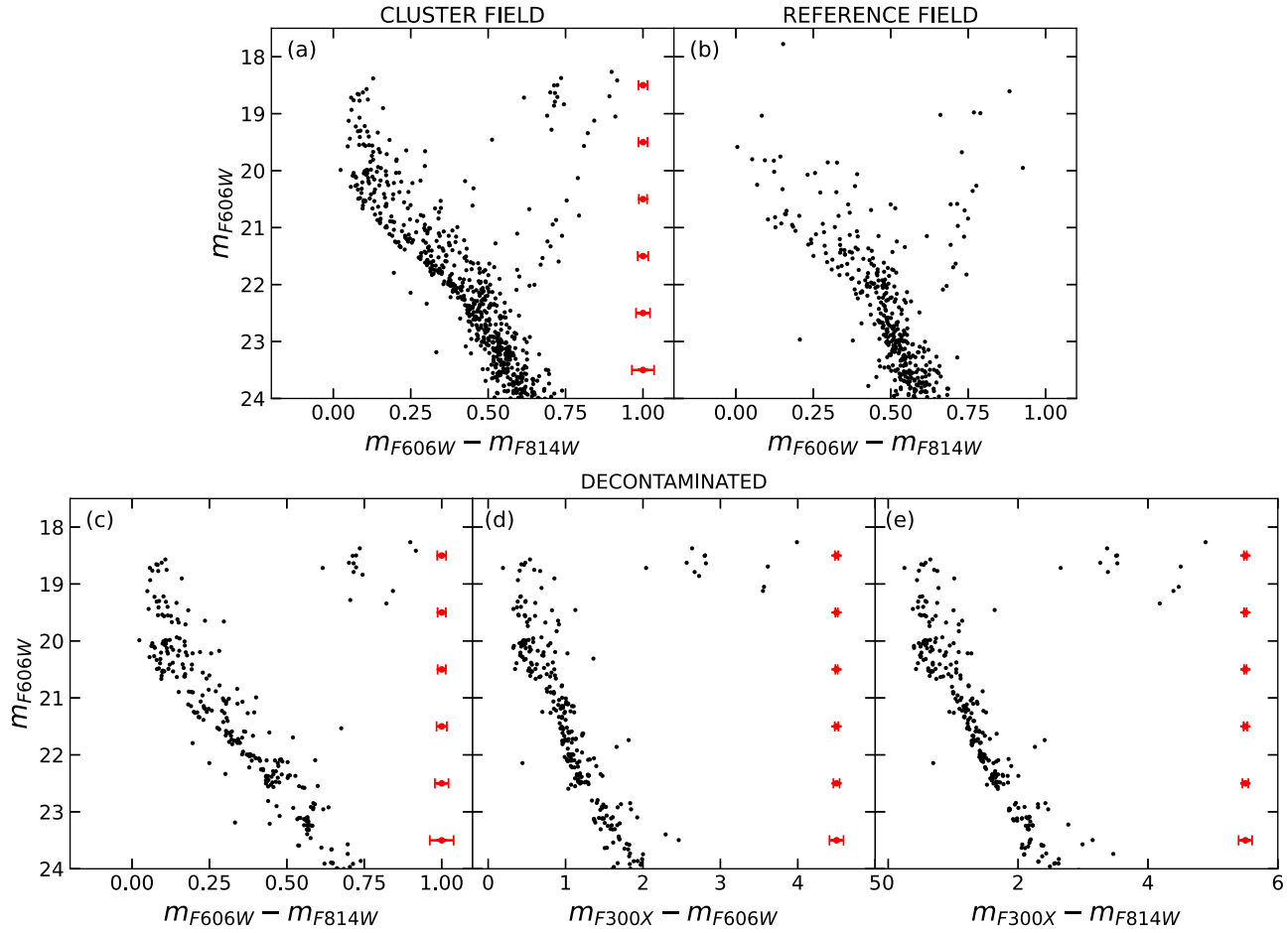

Figure 2. Panel (a): optical CMD of a circular area with a radius of 15″ centered on KMK 88-10. Panel (b): optical CMD of a field region with an equal size area used for decontamination purposes. Panels (c)–(e): decontaminated CMDs of KMK 88-10 in all filter combinations. The typical photometric errors for different magnitude bins are shown in red.

nonrotating stars shows that the stellar population of this cluster is quite young, with an age between 600 Myr and 1 Gyr. In fact, isochrones in this age range nicely reproduce both the MS turnoff region, also accounting for its broadening in color, and the position of the red clump of stars. These results are qualitatively in agreement with those independently obtained by Narloch et al. (2022), who quoted $t \sim 537 \pm 23$ Myr.

3.2. Surface Brightness Profile and Structural Parameters

The very low number of stars in this cluster hampers a characterization of its density profile via number counts (Lanzoni et al. 2007; Ibata et al. 2009; Lanzoni et al. 2010; Miocchi et al. 2013; Cadelano et al. 2017; Lanzoni et al. 2019). Therefore, to constrain its structural properties, we analyzed the surface brightness profile. As a first step, we divided the field of view into concentric radial rings centered on the cluster gravitational center quoted in Bica et al. (2008) and Nayak et al. (2016): α: 05^{h}: 05^{m}: 14^{s}, δ: $-69°$: $22'$: $12''$. Each ring was then divided into four sectors, and the integrated surface brightness of each sector was determined. The average of the values measured among the considered sectors was then adopted as the integrated surface brightness of each ring, while the standard deviation has been assumed as its uncertainty. In this procedure, the portions of the images included within the tidal radius of NGC 1835 were excluded. To properly estimate the background level, we extended the measurement of the surface brightness to the parallel images obtained with the ACS in a region far distant from both clusters. The resulting surface brightness profile obtained in the $m_{\rm F606W}$ filter is shown in Figure 4 (open circles). The profile shows an almost constant value in the most central regions ($r < 4''$), then it smoothly declines toward a plateau at distances of $r > 20''$, where the contamination due to field stars becomes dominant. The average surface brightness of the last three points provided an estimate of the mean background surface brightness ($\mu_{\rm F606W} \sim 21.5$ mag arcsec^{-2}), and this value was subtracted from all of the observed points to obtain the decontaminated profile of KMK 88-10 (filled circles).

The decontaminated profile has the typical shape of the King models (King 1966), which are usually adopted to describe the surface brightness of star clusters. Hence, to determine the structural parameters of KMK 88-10, we fitted the obtained profile with the family of spherical, isotropic, single-mass King models. The comparison was performed through a Monte Carlo Markov Chain fitting technique following the prescriptions by Raso et al. (2020), Cadelano et al. (2022), and Deras et al. (2023). We assumed a χ^2 likelihood and flat priors for all fitting parameters. The resulting best-fit model is shown in Figure 4. It turns out that the cluster is characterized by a King concentration index of about $c = 1.3$, central surface brightness $\mu_{\rm F606W,0} = 19.8$ mag arcsec^{-2}, core radius $r_c = 4\farcs0$, half-mass radius $r_{hm} = 12''$, and tidal radius $r_t = 81''$. By integrating the

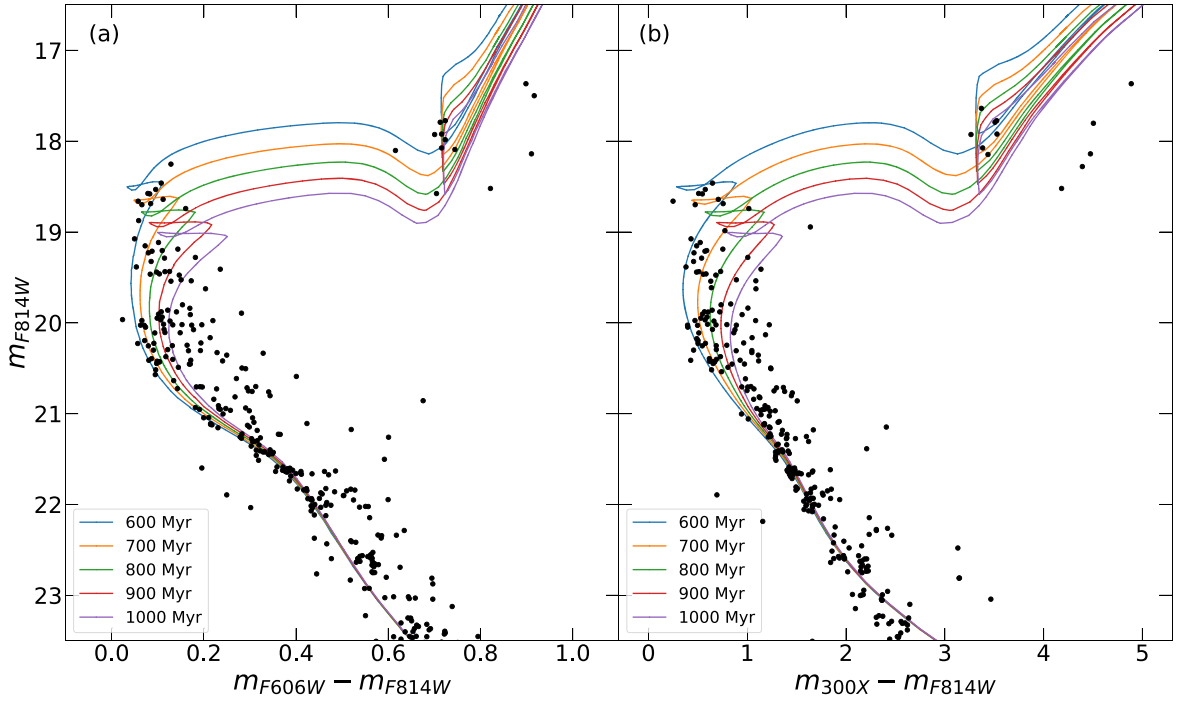

Figure 3. Panel (a): decontaminated optical CMD of KMK 88-10 (black dots) with a set of PARSEC isochrones (Marigo et al. 2017) computed for different ages superposed as colored lines (see the legend). The adopted metallicity is [Fe/H] = −0.4 dex. A distance modulus $(m - M)_0 = 18.48$ and a color excess $E(B - V) = 0.06$ have been assumed to plot the isochrones in the observed CMD. Panel (b): same as panel (a) but in the hybrid m_{F814W} vs. $(m_{F300X} - m_{F814W})$ CMD.

best-fit surface brightness profile, we obtained an integrated magnitude of $m_{F606W,int} = 17.9$. This value, assuming the distance modulus and color excess quoted above, corresponds to an absolute magnitude of $M_{F606W,int} = -0.75$ that, following the prescriptions by Harris (2018), corresponds to an absolute Johnson V-band magnitude of $M_V = -0.71$. Finally, assuming a mass-to-light ratio (M/L_V) of ∼0.5–1, as appropriate for such a young stellar population (Maraston 1998), the total mass is $M \sim 80$–$160\ M_\odot$, compatible with that of a low-mass open cluster (e.g., Piskunov et al. 2008). This value is two to four times smaller than that derived by Popescu et al. (2012), likely because of the different data sets, background decontamination procedure, and mass estimate technique adopted there.

4. A Tidal Bridge between KMK 88-10 and NGC 1835?

Interestingly, the projected distance between the gravitational centers of KMK 88-10 and NGC 1385 ($d = 130''$, corresponding to ∼31 pc) is smaller than the sum of the tidal radii of the two clusters ($r_t \sim 80'' \sim 19$ pc for KMK 88-10, $r_t \sim 105'' \sim 25$ pc for NGC 1835). Moreover, we find that the two systems share similar bulk proper motions. These have been estimated from the Gaia Data Release 3 catalog (Gaia Collaboration et al. 2022) for the stars that survived the decontamination procedure in KMK 88-10 and those located between 15″ and 40″ from the center in NGC 1835 (this selection is intended to minimize the number of contaminating field objects and, at the same time, to exclude low-quality proper-motion measurements in the inner region of such a dense cluster). We obtained a final sample of 34 stars in KMK 88-10 and 246 stars in NGC 1835, from which we calculated the average proper motion in R.A. (μ_α) and decl. (μ_δ) of the two clusters, finding $(\mu_\alpha, \mu_\delta)_{KMK88-10} = (2.12 \pm 0.25, 0.02 \pm 0.27)$ mas yr^{-1} for the former and $(\mu_\alpha, \mu_\delta)_{NGC\ 1835} = (1.93 \pm 0.27, -0.08 \pm 0.30)$ mas yr^{-1} for the latter. Although the statistic is poor, the evidence of a comparable bulk proper motion, together with a small projected distance on the sky, opens up the possibility that the two clusters are gravitationally bound.

To further investigate this hypothesis, we compared the observed separation with the Jacobi radius (r_J) and the Roche-lobe radius (r_{RL}) of NGC 1835. The former has been calculated as (Bertin & Varri 2008 see also Dalessandro et al. 2018)

$$r_J = \left(\frac{GM}{\xi\,\Omega^2}\right)^{1/3}, \quad (1)$$

where G is the gravitational constant, M is the total mass of the cluster, and Ω is its orbital frequency in the host galaxy. Under the assumption that the LMC potential is properly described by a spherical Plummer model with a characteristic radius of $b = 2.6$ kpc (see, e.g., Bekki & Chiba 2005), the dimensionless parameter ξ can be calculated as

$$\xi(R_0) = \frac{3R_0^2}{b^2 + R_0^2}, \quad (2)$$

where R_0 is the radius of the circular orbit (i.e., the galactocentric distance of the cluster). Assuming a total mass $M = 6 \times 10^5\ M_\odot$ (Mackey & Gilmore 2003; McLaughlin & van der Marel 2005), a galactocentric radius $R_0 = 1.56$ kpc (McLaughlin & van der Marel 2005), and an orbital frequency $\Omega = 0.03$ km s^{-1} pc^{-1} (Dalessandro et al. 2018), we find that the Jacobi radius of NGC 1835 is $r_J \sim 155$ pc, which suggests that KMK 88-10 is totally contained (at least in projection) within its gravitational sphere of influence. Finally, the Roche-lobe radius of NGC 1835, calculated following Eggleton (1983) and assuming a mass ratio of ∼1000, turns out to be ∼0.8 times the separation between the two systems ($r_{RL} \sim$ 25 pc), thus indicating that KMK 88-10 extends within it.

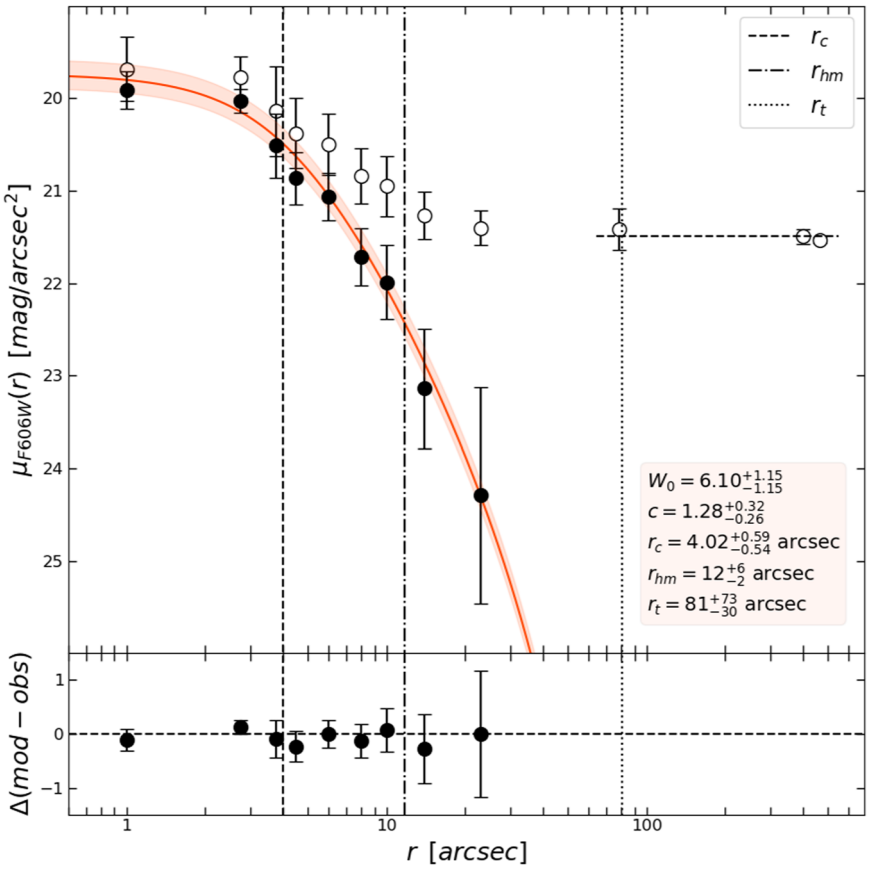

Figure 4. Surface brightness profile of KMK 88-10 in the F606W filter. The open circles represent the observed measures, while the filled circles correspond to the cluster profile after subtraction of the LMC field contribution (horizontal dashed line). The red solid line shows the best-fit King model, with the corresponding structural parameter values labeled in the figure legend. The vertical lines mark the locations of the core (dashed line), half-mass (dotted–dashed line), and tidal (dotted line) radii.

Although both r_J and r_{RL} have been compared with a projected (rather than 3D) distance, it is definitely worth investigating the intriguing possibility that the proximity of these two systems is not merely due to a chance coincidence but to a physical connection. The lack of tidal tails in the observed surface brightness profile of KMK 88-10 is not conclusive in this sense because the largely dominant field contribution in the external region of the system could easily hide this feature. Thus, to test this hypothesis, we created a 2D density map where the severe contamination from field objects is minimized. To this end, we first drew selection boxes enclosing the MS and post-MS stars of KMK 88-10 in its decontaminated CMD (bottom panels of Figure 2) and three additional selection boxes corresponding to the MS, RGB, and horizontal branch sequences of NGC 1835. Then, we selected the stars located across the whole field of view and falling within one of these boxes in the observed CMD. To drastically reduce the contamination from bright field stars, the sample was further refined to include only stars with $m_{F606W} < 20.2$. The 2D density map of this sample was created by gridding the field of view in $1'' \times 1''$ cells and applying a Gaussian kernel to obtain a smoothed distribution. The result is shown in Figure 5, with different colors and lines corresponding to different values of significance (σ) above the background level. The latter is computed as the mean value of the smoothed density distribution in a region far from both clusters, toward the east corner of the sampled field of view (see Figure 1), while σ corresponds to its standard deviation. The map clearly shows

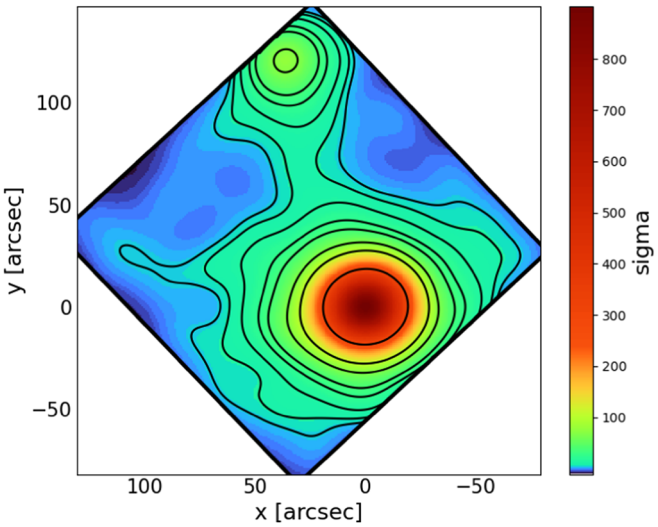

Figure 5. Surface density map of the field sampled by the discussed HST/WFC3 observations, with the same size and orientation as Figure 1. Different colors correspond to different values of significance (σ) above the background level (see the side color bar). The isodensity contour levels (black lines) range from $\sim 4\sigma$ to $\sim 300\sigma$, with irregular steps. The highest density peak corresponds to the location of NGC 1835, while the northern overdensity is KMK 88-10. The presence of a bridge between the two systems is also apparent.

the presence of two overdensities in the north and southwest directions centered on KMK 88-10 and NGC 1835, respectively. Interestingly, the KMK 88-10 density distribution

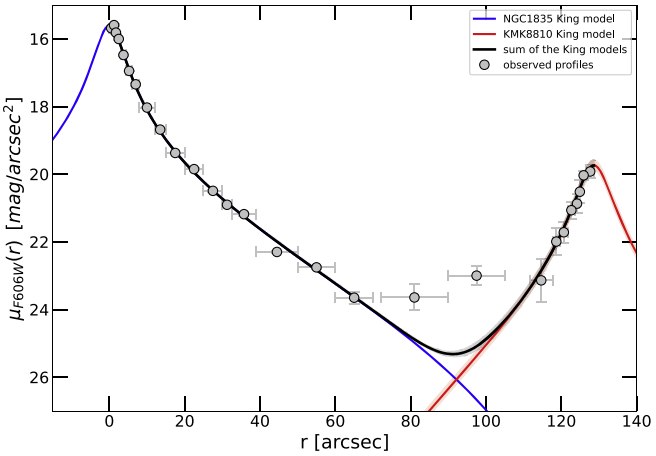

Figure 6. Decontaminated surface brightness profile (gray circles) of NGC 1835 (C. Giusti et al. 2023, in preparation), KMK 88-10 (same as in Figure 4), and the bridge region between them as a function of the distance from the center of the globular cluster. The blue and red lines are the best-fit King models to the profiles of NGC 1835 and KMK 88-10, respectively. The black line is the sum of the two King models.

appears to be nonspherical and elongated toward the direction of NGC 1835. Indeed, the isodensity contours have significant ellipticity, with the major axis directed toward the center of NGC 1835. Furthermore, a small overdensity of stars is present in the region connecting the two clusters, creating a sort of bridge between the two systems. Despite the small number of stars and some residual contamination from field objects, this feature suggests a possible physical connection between the two clusters.

In principle, however, the observed intracluster overdensity could also be due to the mere superposition of the two individual density profiles. To investigate this possibility, we determined the surface brightness profile of NGC 1835 using the same method adopted for KMK 88-10 (see Section 3.2), and we measured the surface brightness distribution in two rectangular regions covering the "bridge area" between the two systems. Since the field level found for NGC 1835 is equal to that observed for KMK 88-10 ($\mu_{F606W} \sim 21.4$ mag arcsec^{-2}; see the horizontal dashed line in Figure 4), this has been used to decontaminate all of the observed surface brightness values from the LMC contribution. The results as a function of the distance from the center of NGC 1835 are shown as gray circles in Figure 6. The red line is the best-fit King model to the surface brightness profile of KMK 88-10 (same as in Figure 4), while the blue line is the same but for NGC 1835 (C. Giusti et al. 2023, in preparation). The black line is the sum of the two profiles. As is apparent, only a very small overdensity of $\mu_{F606W} \sim 25$ is expected at $r \sim 90''$ from the superposition of the surface brightness profiles of the two clusters, while the value measured along the bridge at the same distance is $\sim$2 mag brighter. This indicates that the observed intracluster bridge could indeed be the result of an ongoing interaction between the two systems, where the small cluster KMK 88-10 is being tidally captured by the massive globular cluster NGC 1835. Unfortunately, KMK 88-10 is adjacent to the northern edge of the sampled field of view, thus preventing any detection of the trailing tail expected in the case of a tidal distortion effect. On the other hand, we verified that the bridge is not visible in the density map obtained from stars belonging to NGC 1835 alone (i.e., selected along the MS and RGB of the globular cluster at magnitudes of $m_{F606W} > 20$, where the contribution from KMK 88-10 stars is totally negligible). This indicates that the bridge is primarily composed of KMK 88-10 stars that are gravitationally pulled in by NGC 1835.

Table 1
Summary of the Main Properties of KMK 88-10

Parameter	Estimated Value
Center of gravity	$\alpha_{J2000} = 05^h05^m14^s$ $\delta_{J2000} = -69°22'12''$
Age	$t = 600$ Myr—1 Gyr
King concentration	$c = 1.28^{+0.32}_{-0.26}$
Core radius	$r_c = 4''.02^{+0.59}_{-0.54}$ arcsec (0.97 pc)
Half-mass radius	$r_{hm} = 12^{+6}_{-2}$ arcsec (2.89 pc)
Tidal radius	$r_t = 81^{+73}_{-30}$ arcsec (19.49 pc)
Integrated V magnitude	$M_V = -0.71$
Mass	$M = 80$–$160\ M_\odot$

5. Summary and Conclusions

We used high-resolution HST/WFC3 images to analyze the stellar population of KMK 88-10, a small star cluster located in the LMC. This system lies at an angular separation of approximately 130″ in the sky from the massive and old globular cluster NGC 1835. The adopted data set allowed us to construct the deepest CMD obtained so far for KMK 88-10, properly decontaminated from the strong contribution of LMC field stars. In turn, this allowed a detailed characterization of the stellar population and structural properties of the system.

The decontaminated CMD clearly shows the presence of a young (600–1000 Myr old) stellar population. We detected a significant broadening of the MS turnoff region, suggesting that this stellar system is affected by the same phenomenon observed in many other young LMC clusters, possibly connected to stellar rotation. We also analyzed the surface brightness profile of the cluster and fit it with a King model. Under the assumption of a distance modulus $(m - M)_0 = 18.48$, we found a core radius of 0.97 pc, half-mass radius of 2.89 pc, and concentration parameter of $c \sim 1.3$, corresponding to a truncation radius of about 19 pc. The integration of the best-fit surface brightness profile provides an integrated V-band absolute magnitude of $M_V = -0.71$, corresponding to a mass $M \sim 80$–$160\ M_\odot$ for a mass-to-light ratio $(M/L_V) \sim 0.5$–1. The main physical parameters of the cluster are summarized in Table 1.

At the LMC distance, the small angular separation between KMK 88-10 and NGC 1835 (130″) corresponds to a projected physical distance of only $\sim$30 pc, which is smaller than the sum of the two tidal radii and the Jacobi radius of the globular cluster. In addition, KMK 88-10 turns out to extend within the Roche-lobe radius of NGC 1835. Although the 3D distance is likely larger than the projected one, the observed proximity promoted the investigation of a possible physical link between the two systems. With this purpose, we constructed a 2D surface density map of the likely cluster members surveyed in the WFC3 field of view, finding that KMK 88-10 has an elongated structure toward the direction of NGC 1835 (see Figure 5). Furthermore, an overdensity between the two clusters significantly exceeding the superposition of the two surface brightness profiles has been detected, suggesting the presence of a tidal bridge between the two systems. If confirmed, this would be the first evidence of a globular cluster caught in the act of tidally capturing a young low-mass

star cluster. According to our mass estimate for KMK 88-10 and the value quoted by Mackey & Gilmore (2003) and McLaughlin & van der Marel (2005) for NGC 1835, the two interacting stellar systems would have an extremely high mass ratio ($M_{\rm NGC\ 1835}/M_{\rm KMK\ 88-10} \sim 6 \times 10^3$). As discussed above, such events are supposed to be quite rare and have a significant impact on the evolution and observed characteristics of massive star clusters. Indeed, cluster mergers could explain the properties of massive and dynamically complex systems (e.g., Baumgardt et al. 2003; Brüns & Kroupa 2011) and provide an explanation for the presence of the light-element complexities in LMC intermediate-age clusters (Hong et al. 2017) and multiple iron distribution in some old clusters (Gavagnin et al. 2016). The final fate of this interaction should lead to the tidal destruction of KMK 88-10 in a timescale that depends on its orbit, possibly leaving an observable kinematical signature due to the dynamical heating of the stars in the outer regions of NGC 1835. This could be observable through a rise in the stellar velocity dispersion in the cluster outskirts. Hence, spectroscopic observations aimed at measuring the stellar velocity dispersion profile of NGC 1835 might shed light on this and help confirm the tidal capture scenario.

Acknowledgments

This work is part of the project *Cosmic-Lab* (*"Globular Clusters as Cosmic Laboratories"*) at the Physics and Astronomy Department "A. Righi" of the Bologna University (http://www.cosmic-lab.eu/Cosmic-Lab/Home.html). The research was funded by the MIUR through the PRIN-2017 grant awarded to the project Light-on-Dark (PI: Ferraro) with contract PRIN-2017K7REXT.

Facilities: HST(WFC3), HST(ACS).

ORCID iDs

Camilla Giusti https://orcid.org/0000-0002-7717-1022
Mario Cadelano https://orcid.org/0000-0002-5038-3914
Francesco R. Ferraro https://orcid.org/0000-0002-2165-8528
Barbara Lanzoni https://orcid.org/0000-0001-5613-4938
Silvia Leanza https://orcid.org/0000-0001-9545-5291
Cristina Pallanca https://orcid.org/0000-0002-7104-2107
Enrico Vesperini https://orcid.org/0000-0003-2742-6872
Emanuele Dalessandro https://orcid.org/0000-0003-4237-4601
Alessio Mucciarelli https://orcid.org/0000-0001-9158-8580

References

Amaro-Seoane, P., Konstantinidis, S., Brem, P., et al. 2013, MNRAS, 435, 809
Baumgardt, H., Makino, J., Hut, P., et al. 2003, ApJL, 589, L25
Baumgardt, H., Parmentier, G., Anders, P., et al. 2013, MNRAS, 430, 676
Bekki, K., & Chiba, M. 2005, MNRAS, 356, 680
Bellini, A., Anderson, J., & Bedin, L. R. 2011, PASP, 123, 622
Bertin, G., & Varri, A. L. 2008, ApJ, 689, 1005
Bhatia, R. K., & Hatzidimitriou, D. 1988, MNRAS, 230, 215
Bhatia, R. K., Read, M. A., Hatzidimitriou, D., et al. 1991, A&AS, 87, 335
Bica, E., Bonatto, C., Dutra, C. M., et al. 2008, MNRAS, 389, 678
Brocato, E., Castellani, V., Ferraro, F. R., et al. 1996, MNRAS, 282, 614
Brüns, R. C., & Kroupa, P. 2011, ApJ, 729, 69
Cadelano, M., Chen, J., Pallanca, C., et al. 2020, ApJ, 905, 63
Cadelano, M., Dalessandro, E., Ferraro, F. R., et al. 2017, ApJ, 836, 170
Cadelano, M., Dalessandro, E., Salaris, M., et al. 2022, ApJL, 924, L2
Cadelano, M., Dalessandro, E., Webb, J. J., et al. 2020, MNRAS, 499, 2390
Cadelano, M., Ferraro, F. R., Dalessandro, E., et al. 2022, ApJ, 941, 69
Cadelano, M., Ferraro, F. R., Istrate, A. G., et al. 2019, ApJ, 875, 25
Choudhury, S., Subramaniam, A., & Piatti, A. E. 2015, AJ, 149, 52
Dalessandro, E., Ferraro, F. R., Bastian, N., et al. 2019, A&A, 621, A45
Dalessandro, E., Zocchi, A., Varri, A. L., et al. 2018, MNRAS, 474, 2277
Darma, R., Arifyanto, M. I., & Kouwenhoven, M. B. N. 2021, MNRAS, 506, 4603
de la Fuente Marcos, R., & de la Fuente Marcos, C. 2010, ApJ, 719, 104
de la Fuente Marcos, R., de la Fuente Marcos, C., & Reilly, D. 2014, Ap&SS, 349, 379
de Oliveira, M. R., Bica, E., & Dottori, H. 2000, MNRAS, 311, 589
de Oliveira, M. R., Dottori, H., & Bica, E. 1998, MNRAS, 295, 921
De Silva, G. M., Carraro, G., D'Orazi, V., et al. 2015, MNRAS, 453, 106
Deras, D., Cadelano, M., Ferraro, F. R., et al. 2023, ApJ, 942, 104
Dieball, A., Müller, H., & Grebel, E. K. 2002, A&A, 391, 547
Eggleton, P. P. 1983, ApJ, 268, 368
Ferraro, F. R., Fusi Pecci, F., Testa, V., et al. 1995, MNRAS, 272, 391
Ferraro, F. R., Lanzoni, B., Dalessandro, E., et al. 2012, Natur, 492, 393
Ferraro, F. R., Lanzoni, B., Dalessandro, E., et al. 2019, NatAs, 3, 1149
Ferraro, F. R., Lanzoni, B., & Dalessandro, E. 2020, RLSFN, 31, 19
Ferraro, F. R., Lanzoni, B., Raso, S., et al. 2018, ApJ, 860, 36
Ferraro, F. R., Lanzoni, B., Vesperini, E., et al. 2023, ApJ, 950, 145
Ferraro, F. R., Mucciarelli, A., Carretta, E., et al. 2006, ApJL, 645, L33
Ferraro, F. R., Origlia, L., Testa, V., et al. 2004, ApJ, 608, 772
Gaia Collaboration, Vallenari, A., Brown, A. G. A., et al. 2023, A&A, 674, A1
Gavagnin, E., Mapelli, M., & Lake, G. 2016, MNRAS, 461, 1276
Glatt, K., Grebel, E. K., & Koch, A. 2010, A&A, 517, A50
Harris, J., & Zaritsky, D. 2009, AJ, 138, 1243
Harris, W. E. 2018, AJ, 156, 296
Hong, J., de Grijs, R., Askar, A., et al. 2017, MNRAS, 472, 67
Ibata, R., Bellazzini, M., Chapman, S. C., et al. 2009, ApJL, 699, L169
Kamann, S., Bastian, N., Gossage, S., et al. 2020, MNRAS, 492, 2177
King, I. R. 1966, AJ, 71, 64
Lanzoni, B., Dalessandro, E., Ferraro, F. R., et al. 2007, ApJL, 668, L139
Lanzoni, B., Ferraro, F. R., Alessandrini, E., et al. 2016, ApJL, 833, L29
Lanzoni, B., Ferraro, F. R., Dalessandro, E., et al. 2010, ApJ, 717, 653
Lanzoni, B., Ferraro, F. R., Dalessandro, E., et al. 2019, ApJ, 887, 176
Lee, Y.-W., Joo, J.-M., Sohn, Y.-J., et al. 1999, Natur, 402, 55
Leon, S., Bergond, G., & Vallenari, A. 1999, A&A, 344, 450
Mackey, A. D., & Broby Nielsen, P. 2007, MNRAS, 379, 151
Mackey, A. D., & Gilmore, G. F. 2003, MNRAS, 338, 85
Maraston, C. 1998, MNRAS, 300, 872
Marigo, P., Girardi, L., Bressan, A., et al. 2017, ApJ, 835, 77
Martocchia, S., Bastian, N., Saracino, S., et al. 2023, MNRAS, 520, 4080
McLaughlin, D. E., & van der Marel, R. P. 2005, ApJS, 161, 304
Milone, A. P., Marino, A. F., Di Criscienzo, M., et al. 2018, MNRAS, 477, 2640
Miocchi, P., Lanzoni, B., Ferraro, F. R., et al. 2013, ApJ, 774, 151
Mucciarelli, A., Carretta, E., Origlia, L., et al. 2008, AJ, 136, 375
Mucciarelli, A., Massari, D., Minelli, A., et al. 2021, NatAs, 5, 1247
Mucciarelli, A., Origlia, L., Ferraro, F. R., et al. 2006, ApJ, 646, 939
Mucciarelli, A., Origlia, L., & Ferraro, F. R. 2010, ApJ, 717, 277
Mucciarelli, A., Origlia, L., Ferraro, F. R., et al. 2012, ApJL, 746, L19
Narloch, W., Pietrzyński, G., Gieren, W., et al. 2022, A&A, 666, A80
Nayak, P. K., Subramaniam, A., Choudhury, S., et al. 2016, MNRAS, 463, 1446
Olsen, K. A. G., Hodge, P. W., Mateo, M., et al. 1998, MNRAS, 300, 665
Palma, T., Clariá, J. J., Geisler, D., et al. 2013, A&A, 555, A131
Palma, T., Gramajo, L. V., Clariá, J. J., et al. 2016, A&A, 586, A41
Piatti, A. E. 2012, A&A, 540, A58
Piatti, A. E., Guandalini, R., Ivanov, V. D., et al. 2014, A&A, 570, A74
Pietrzyński, G., Graczyk, D., Gallenne, A., et al. 2019, Natur, 567, 200
Pietrzynski, G., & Udalski, A. 2000, AcA, 50, 337
Piskunov, A. E., Schilbach, E., Kharchenko, N. V., et al. 2008, A&A, 477, 165
Popescu, B., Hanson, M. M., & Elmegreen, B. G. 2012, ApJ, 751, 122
Portegies Zwart, S. F., & Rusli, S. P. 2007, MNRAS, 374, 931
Priyatikanto, R., Arifyanto, M. I., Darma, R., et al. 2019, in IAU Symp. 344, Dwarf Galaxies: From the Deep Universe to the Present (Cambridge: Cambridge Univ. Press), 118
Priyatikanto, R., Ikbal Arifyanto, M., Wulandari, H. R. T., et al. 2019, JPhCS, 1127, 012053
Priyatikanto, R., Kouwenhoven, M. B. N., Arifyanto, M. I., et al. 2016, MNRAS, 457, 1339
Rao, P. D., Ramamani, N., & Alladin, S. M. 1987, BASI, 15, 43
Raso, S., Libralato, M., Bellini, A., et al. 2020, ApJ, 895, 15
Stetson, P. B. 1987, PASP, 99, 191
Stetson, P. B. 1994, PASP, 106, 250
Subramaniam, A., Gorti, U., Sagar, R., et al. 1995, A&A, 302, 86
Vallenari, A., Bettoni, D., & Chiosi, C. 1998, A&A, 331, 506
van den Bergh, S. 1996, ApJL, 471, L31
Wenger, M., Ochsenbein, F., Egret, D., et al. 2000, A&AS, 143, 9